Int. J. Electrochem. Sci., 7 **(2012)** 7976 - 7983

International Journal of
ELECTROCHEMICAL
SCIENCE
www.electrochemsci.org

A Comparative Study of Nanoparticles and Nanospheres $ZnFe_2O_4$ as Anode Material for Lithium Ion Batteries

Huayun Xu, Xianglan Chen, Liang Chen, Li'e Li, Liqiang Xu, Jian Yang[*], *Yitai Qian*

Shandong Univ, Key Lab Colloid & Interface Chem, Minist Educ, Sch Chem & Chem Engn, Jinan 250100, Peoples R China
[*]E-mail: xuhuayun@sdu.edu.cn

Received: 9 July 2012 / *Accepted:* 30 July 2012 / *Published:* 1 September 2012

Spinel structure $ZnFe_2O_4$ were prepared by hydrothermal and solvothermal methods. Investigations on X-ray diffraction (XRD) and transmission electron microscopy (TEM) indicate that the samples are well-crystallized cubic $ZnFe_2O_4$ with average nanoparticle size ranging from 30 to 90 nm and nanosphere size in the range of 200~250 nm composed of around 20 nm nanoparticles with increasing sintered temperature for hydrothermal and solvothermal method, respectively. The $ZnFe_2O_4$ samples sintered at 600 ^oC show high lithium-storage capacity and good reversibility. Compared with nanoparticles, $ZnFe_2O_4$ nanospheres demonstrate a reversible capacity over 860 mAh g^{-1} and good rate capability. Electrochemical impedance spectroscopy (EIS) was carried out and decreased warburg impedance was found for nanospheres compared to nanoparticle $ZnFe_2O_4$.

Keywords: $ZnFe_2O_4$; Nanostructured materials; Lithium ion battery; Electrochemical impedance spectroscopy

1. INTRODUCTION

Lithium-ion batteries are widely used in consumer electronic devices and a lot of anode materials have been investigated such as carbon materials which have been widely used in commercially available lithium ion batteries (LIBs) based on the low cost, long cycle life and environment-friendly nature [1–5]. However, carbon materials can't meet the demand for higher energy density of lithium ion battery due to a low specific capacity (theoretical capacity: 372 mAh g^{-1}). Hence the development of novel anode materials for high specific capacity compared with the conventional carbon materials is important.

Transition metal oxides such as Fe_3O_4 [6, 7] and ferrites with general formula AFe_2O_4 (A: Zn, Ni, Co, Cu, Cd) [8–16] have been widely investigated as promising anode materials for high-power lithium-ion batteries due to their relatively high theoretical capacities (600~1000 mAh g^{-1}). Among them, $ZnFe_2O_4$ shows a high reversible capacity (theoretical capacity: 1072 mAh g^{-1}, according to 9 moles Li per mole of $ZnFe_2O_4$) because Zn can contribute additional capacity due to alloying-de-alloying reaction besides buffering the volume variation during conversion reaction [12, 13, 17, 18]. But it suffers from structure instability owing to volume change during charge /discharge course, low electron conductivity and aggregation of the particles caused by charge/discharge cycles [19]. As we know, nanoscale structure can effectively shorten Li^+ insertion/extraction pathways and morphology of electrode material plays an important role on the electrochemical performance for Li-ion batteries [12, 19-21]. Chen synthesized hollow sphere ~1μm in diameter shows reversible capacity 900 mAh [12]. Nuli reported nanofilm $ZnFe_2O_4$ by laser deposit method retaining reversible capacity of 432 mAh g^{-1} g after 100 cycles [19]. Chowdari found cubic $ZnFe_2O_4$ with a particle size range of 100~300 nm obtained by urea combustion performs 615 mAh g^{-1} after 50 cycles [21].

In our work, we synthesized cubic $ZnFe_2O_4$ by hydrothermal and solvothermal method and investigated the structure and morphology by XRD and TEM. Electrochemical performance tests and EIS were carried out and improved cycling capability and decreased warburg impedance were found for nanospheres $ZnFe_2O_4$ compared to nanoparticles $ZnFe_2O_4$.

2. EXPERIMENTAL

2.1 Synthesis

All reagents were analytical grade and used without further purification. 2 mmol $FeCl_3 \cdot 6H_2O$ and 1 mmol $ZnCl_2$ were mixed under vigorously stirring and adjusted pH by NaOH solution to 9. Then transferred to a Teflon-lined stainless steel autoclave (60 mL) and heated at 200 ^oC for 24 h. The product was collected by centrifugation, washed with distilled water and ethanol, and dried at 80 ^oC in air for 8 h. Finally the powders were annealed at 500 ^oC, 600 ^oC and 700 ^oC for 3 h. For solvothermal method, the difference is using ethyl alcohol as solvent and adding 10 mmol urea into the $FeCl_3 \cdot 6H_2O$ and $ZnCl_2$ solution instead of controlling pH using NaOH solution.

2.2. Characterization

XRD patterns of the samples were provided using a Bruker D8 advanced X-ray diffractometer with Cu Kα radiation (λ=1.5418 Å). The $ZnFe_2O_4$ samples were observed on a transmission electron microscope (TEM, JEOL-2010). The coin cells comprised of the prepared powder as cathode, lithium as anode, and an electrolyte having 1M $LiPF_6$ in an ethylene carbonate (EC)-diethyl carbonate (DEC)-ethyl methyl carbonate (EMC) mixture (1:1:1). Micro-porous polypropylene separator was used in those cells. The cell preparation was carried out in an Ar-filled dry box. The charge/discharge cycles for assembled cells were measured using a Land CT2001 battery tester. EIS were performed by a

Zahner Elektrik IM6 (Germany) impedance instrument over the frequency range of 100 kHz to 0.01Hz.

3. RESULTS AND DISCUSSION

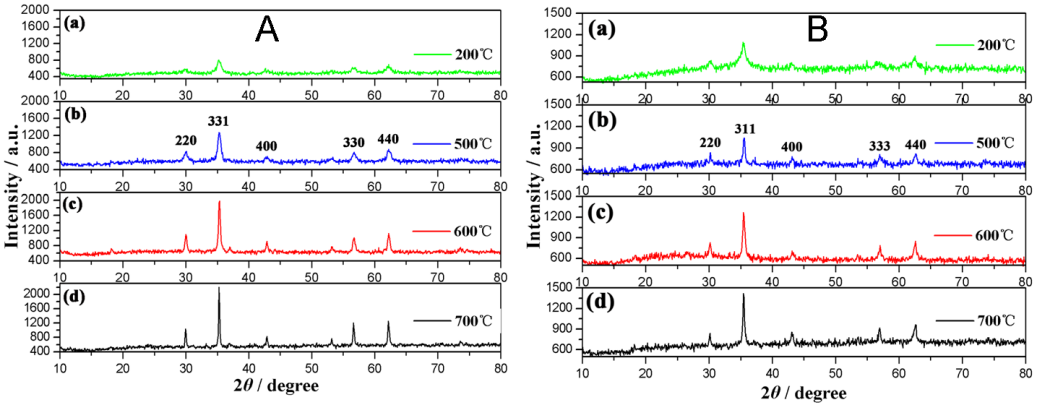

Figure 1. XRD patterns of the $ZnFe_2O_4$ as prepared samples and then sintered at different temperature samples synthesized by hydrothermal (A) and solvothermal method (B)

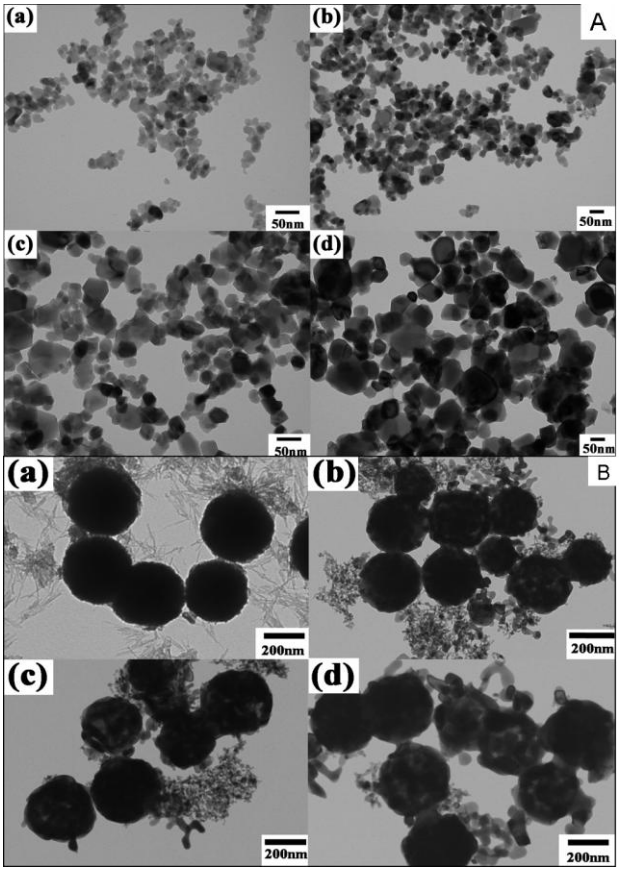

Figure 2. TEM of the $ZnFe_2O_4$ as prepared samples (a) and then sintered at different temperature samples synthesized (b: 500 ^oC, c: 600 ^oC and d: 700 ^oC) by hydrothermal (A) and solvothermal method (B)

XRD analysis (Figure 1A and 1B) indicates that the powders by two routes sintered at 500~700 ^{o}C is phase-pure cubic $ZnFe_2O_4$ (JCPDS card No. 65-3111). It is obvious that with increasing the calcination temperature, the peak becomes sharp which means strengthened crystallization.

Figure 2 shows the TEM of the $ZnFe_2O_4$ as prepared and then sintered at different temperature samples synthesized by hydrothermal (Figure 2A) and solvothermal method (Figure 2B). As shown in Figure 2A, the powder obtained from hydrothermal method are composed by agglomerated nanoparticles with average size ranging from 30 nm to 90 nm around with the increasing sintered temperature. Similar morphology was also reported by polymer pyrolysis method and sol–gel auto-combustion method [21, 22]. TEM imaging (Figure 2B) demonstrates that the powder synthesized by solvothermal method are composed of well-dispersed spheres around 200 nm in diameter and the size of its primary particles is changed from less than 10 nm to around 20 nm. On the other hand, based on Scherrer formula, we calculated the grain size of $ZnFe_2O_4$ to be 24 nm around for powder obtained from solvothermal route, which is consistent with TEM result. It is also can be seen that with increased sintering temperature, the very thin nanofibers and small nanoparticles gradually disappears and becomes the ingredients of nanophere.

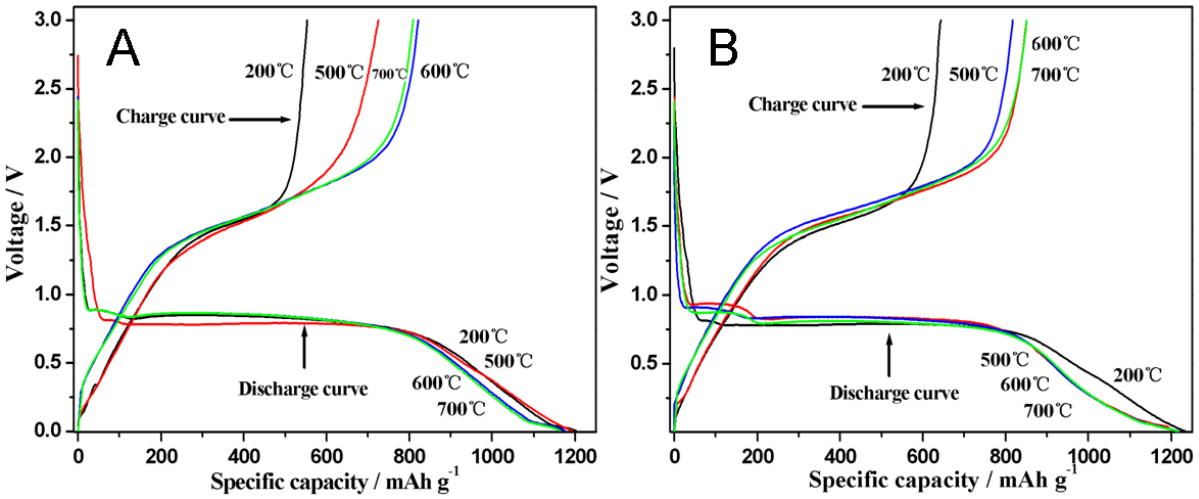

Figure 3. The first charge-discharge curve for as prepared $ZnFe_2O_4$ and then sintered at different temperature samples synthesized by hydrothermal (A) and solvothermal method (B)

Figure 3 shows the initial charge and discharge profile for as prepared $ZnFe_2O_4$ and then sintered at different temperature samples synthesized by hydrothermal (Figure 3A) and solvothermal method (Figure 3B) tested at 50 mA g^{-1} between 0.005-3.0V. It is clear that the initial discharge capacity for all $ZnFe_2O_4$ samples is around 1200 mAh g^{-1}. It is high than 1072 mAh g^{-1} according to 9 lithium insertion, which might be attributed to the nature of the material and the formation of a solid electrolyte interphase (SEI) on the electrode surface due to the decomposition of the electrolyte [23].

Figure 4 shows the discharge capacity as a function of cycle for as prepared $ZnFe_2O_4$ and then sintered at different temperature samples synthesized by hydrothermal (Figure 4A) and solvothermal method (Figure 4B).

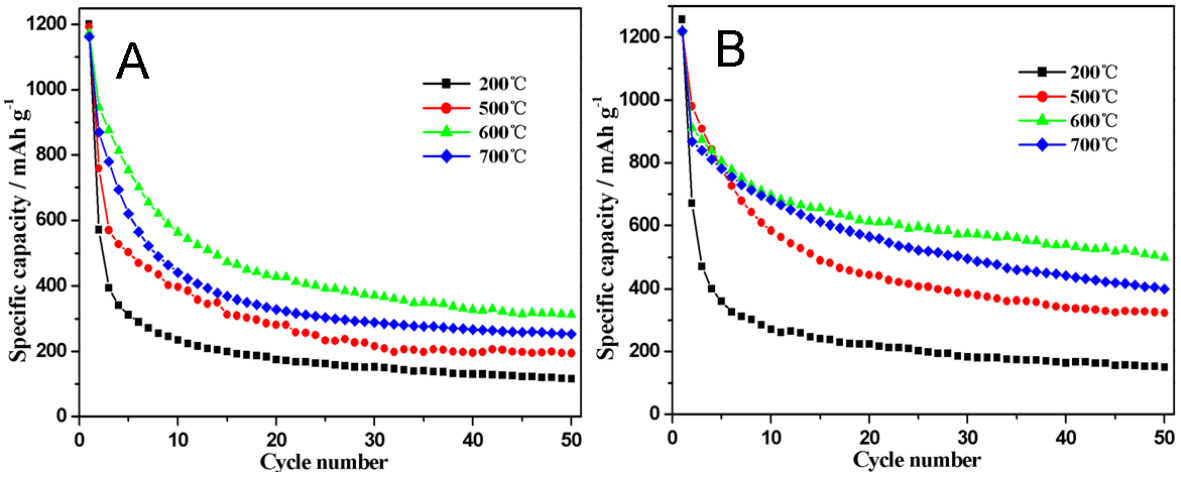

Figure 4. Discharge capacity as a function of cycle for as prepared $ZnFe_2O_4$ and hen sintered at different temperature samples synthesized by hydrothermal (A) and solvothermal method (B)

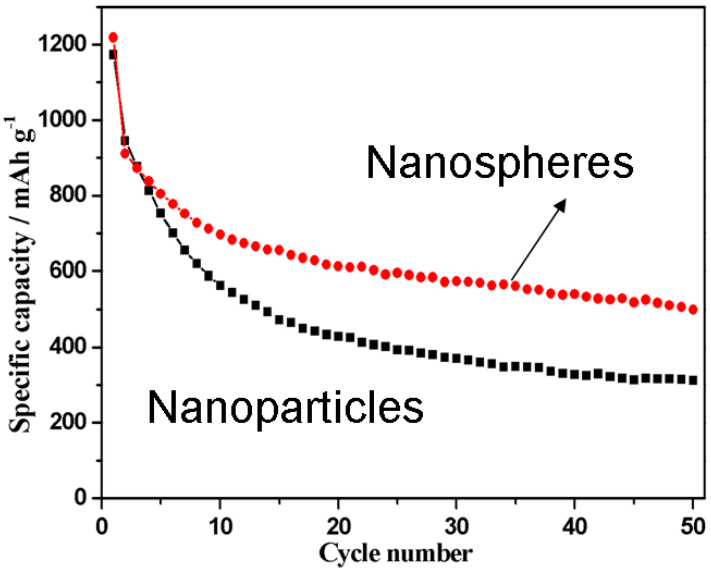

Figure 5. The discharge capacity as a function of cycle for 600 ^oC sample obtained by different method

The tested current is 50 mA g^{-1} and cut-off voltage is between 0.005-3.0V. Sample sintered at 600 ^oC obtained respectively from two different routes show the highest capacity and the best cycle performance. Comparing the cycle performance for 600 ^oC sintered sample obtained by two different methods as shown in Figure 5, it is obvious that the capacity maintaining for nanospheres is much better than that of nanoparticles. After 50 cycles, the capacity of nanospheres is over 500 mAh g^{-1}, while only around 300 mAh g^{-1} was maintained for nanoparticles $ZnFe_2O_4$. Though the capacity behavior is not as good as published results [12, 21], it is expected that the electrochemical performance after carbon material modified could be improved. And in our experiment, it is thought

that nanospheres composed by small nanoparticles are contributed to the structure stability by impress the volume changes during charge and discharge course.

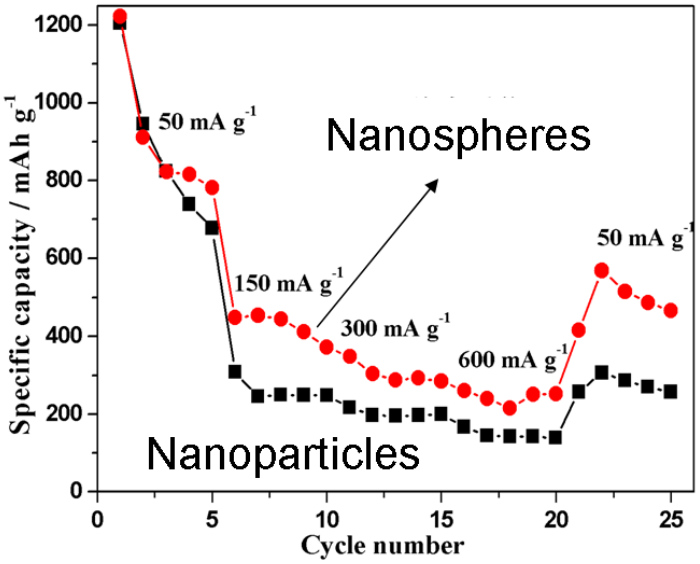

Figure 6. Rate capacity of 600 °C samples obtained by different methods between 0.005 and 3.0 V at various current densities

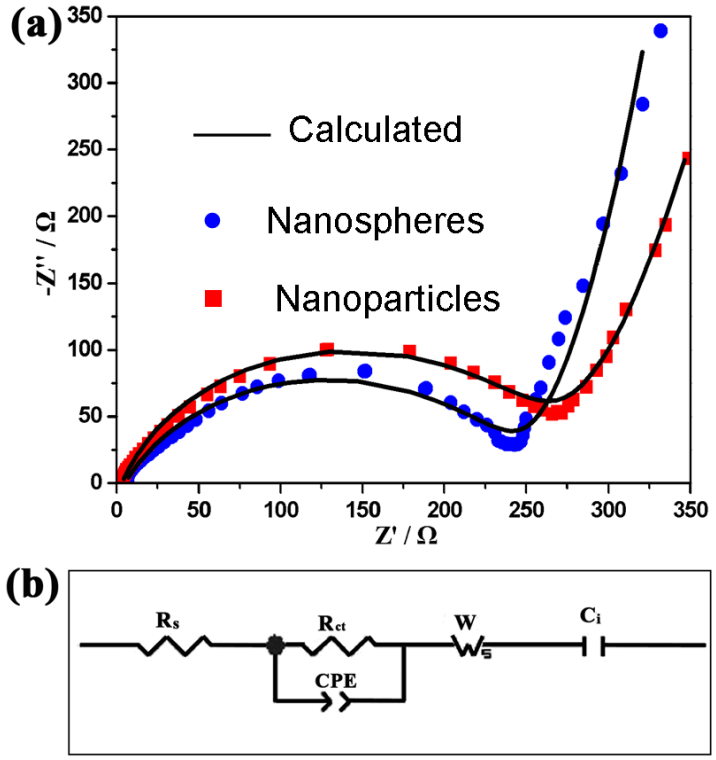

Figure 7. Electrochemical impedance data (red dot: nanoparticles, blue dot: nanospheres) and the fitted curve (black points) of the samples measured at potential of the open circuit voltage (a); the equivalent circuit for modeling the impedance data (b).

Figure 6 shows the rate capacity of 600 ^{o}C samples obtained by different method between 0.005 and 3.0 V at various current densities. $ZnFe_2O_4$ nanospheres perform higher capacity at various current densities from 50 mA g^{-1} to 600 mA g^{-1} compared to nanoparticles. Moreover, when the current density decreases to 50 mA g^{-1} again, nanospheres show more reversible than nanoparticles do, which is believed that $ZnFe_2O_4$ nanospheres composed of small nanoparticles (Figure 2B) are contributed to the structure maintaining during conversion reaction.

Table 1. R_s, R_{ct} and Z_w value of the $ZnFe_2O_4$ nanoparticles and nanospheres

$ZnFe_2O_4$	R_s / Ω	R_{ct} / Ω	W / Ω·cm^{-2}
Nanoparticles	**4.4**	**249.7**	**233.4**
Nanospheres	**5.0**	**234.5**	**115.2**

EIS was performed to investigate the electrode resistance information for 600 ^{o}C sintered samples obtained by two different methods as presented in Figure 7a. The equivalent circuit for modeling impedance data is shown in Figure 7b. The intercept at the real (Z') axis in high frequency corresponds to the ohmic resistance (R_e). The semicircle in the middle frequency range indicates the charge transfer resistance (R_{ct}) and the inclined straight line relates to the Warburg impedance (Z_w). The fitting results are presented in Table 1. The R_{ct} value of the $ZnFe_2O_4$ nanoparticles and nanospheres is 249.7Ω and 234.5 Ω, respectively. The Z_w value for nanoparticles is 233.4 Ω, while only 155.2 Ω for nanospheres. Clearly, the nanospheres $ZnFe_2O_4$ can suppress the warburg impedance which related to lithium ion diffusion in the solid state electrode material. Decreased warburg impedance means faster lithium ion diffusion for nanospheres compared to nanoparticle and then contributed to a higher discharge capacity and rate capability compared to the nanoparticles $ZnFe_2O_4$ (shown in Figure 5 and 6).

4. CONCLUSION

In summary, hydrothermal and solvethermal methods have been developed to prepare $ZnFe_2O_4$ spinel material. Comparing the structure, morphology and electrochemical performance, it is found that nanospheres via solvethermal route performs higher specific capacity, improved cyclability and good rate capability compared to nanoparticles obtained from hydrothermal method. It is believed that the morphology of nanopheres composed of small nanoparticles is contributed to good electrochemical performance for $ZnFe_2O_4$ anode material. $ZnFe_2O_4$ nanospheres show high first discharge and charge capacities of 1215 and 851 mAh g^{-1} at 50 mA g^{-1}. This $ZnFe_2O_4$ represents a promising candidate for

anode material in LIBs, and further improvement by carbon materials such as graphene for nanopheres $ZnFe_2O_4$ is under investigation in our work.

ACKNOWLEDGEMENTS
This study was supported by the 973 Project of China (No.2011CB935901), the National Natural Science Foundation of China (Grant No. 11179043, No. 91022033), the Independent Innovation Foundations of Shandong University (2011GN032, 2012ZD007), Shandong Provincial Natural Science Foundation for Distinguished Young Scholar and start-up funding for new faculties in Shandong University. We are also grateful to the Graduate Independent Innovation Foundation of Shandong University (yzc11034).

References

1. S.L. Yang, H.H. Song, X.H. Chen, *J. Power Sources* 173 (2007) 487-494.
2. Y.S. Wu, Y.H. Wang, Y.H. Lee, *J. Alloy. Compd*. 426 (2006) 218-222.
3. D. Guerard, R.. Janot, J.Ghanbaja, P. Delcroix, *J. Alloy. Compd*. 434 (2007) 410-414.
4. M.S. Sh, F. Golestani, H.Sarpoolaky, *J. Alloy. Compd*. 482 (2009) 361-365.
5. M.A.Worsley,S.O.Kucheyev,J.H.Satcher,A.V.Hamza,T.F. Baumann, *Appl. Phys. Lett*. 94 (2009) 73-77.
6. L. Taberna, S. Mitra, P. Poizot, P. Simon, J.M. Tarascon *Nat. Mater*. 5 (2006) 567-573.
7. S.B. Ni, D.Y. He, X.L. Yang, *J. Alloy. Compd*. 509 (2011) L305-L307.
8. R. Alcántara, M. Jaraba, P. Lavela, J. L. Tirado, J. C. Jumas, J. Olivier-Fourcade, *Electrochem. Commun.* 5 (2003) 16-21.
9. Y. Q. Chu, Z. W. Fu, Q. Z. Qin, *Electrochim. Acta* 49 (2004**)** 4915-4921.
10. M. Bomio, P. Lavela, J. L. Tirado, *J. Solid State Electrochem*. 12 (2008) 726-731.
11. C. Q. Hu, Z. H. Gao, X. R. Yang, *J. Magn. Magn. Mater*. 320 (2008) L70-L73.
12. X. Guo, X. Lu, X. Fang, Y. Mao, Z. Wang, L. Chen, X. Xu, H. Yang, *Electrochem. Commun*. 12 (2010) 847-850.
13. Y. Sharma, N. Sharma, G.V. Subba Rao, B.V.R. Chowdari, *Electrochim. Acta* 53 (2008) 2380-2385.
14. P. Lavela, J.L. Tirado, *J. Power Sources* 172 (2007) 379-387.
15. R. Kalai Selvan, N. Kalaiselvi, C.O. Augustin, C.H. Doh, C. Sanjeeviraja *J. Power Sources* 157 (2006) 522-527.
16. Y. Sharma, N. Sharma, G.V. Subba Rao, B.V.R. Chowdari *Bull Mater Sci* 32 (2009) 295-304.
17. Y. Sharma, N. Sharma, G.V. Subba Rao, B.V.R. Chowdari, *Adv. Funct. Mater*. 17 (2007) 2855-2861.
18. Y. Yang, Y Zhao, L. Xiao, L. Zhang *Electrochem. Commun*. 10 (2008) 1117-1120.
19. Y. N. NuLi, Y. Q. Chu, Q. Z. Qin, *J. Electrochem. Soc.* 151 (2004) A1077-A1083.
20. L. M. Jin, Y. C. Qin, H. Deng, W. S. Li, H. Li, S. H. Yang, *Electrochim. Acta* 56 (2011) 9127-9132.
21. C.T. Cherian, M. V. Reddy, G. V. S. Rao C.H. Sow, B.V.R. Chowdari, *J. Solid State Electrochem* 16 (2012) 1823-1832.
22. Y. Ding, Y.F. Yang, H.X.Shao, *Electrochim. Acta* 56 (2011) 9433-9438.
23. Y. F. Deng, Q. M. Zhang, S. D. Tang, L. T. Zhang, S. N. Deng, Z. C. Shi, G. H. Chen, *Chem. Commun.* 47 (2011) 6828-6830.